Performance analysis and sizing guidelines of electrically-powered extraterrestrial rovers

Performance Analysis and Sizing Guidelines of Electrically-Powered Extraterrestrial Rovers

Giulio Avanzini[a,1], Emanuele L. de Angelis[*,b,2], Fabrizio Giulietti[b,3]

[a] *University of Salento, Lecce, Italy 73100*
[b] *University of Bologna, Forlì, Italy 47121*

Abstract

The paper describes an analytical and experimental framework which investigates performance of electrically-driven ground vehicles powered by battery packs, with the objective of providing simple indications for preliminary sizing of rovers designed for mission on the surface of extraterrestrial bodies. For this class of missions, power is at a premium, and energy-efficient locomotion is clearly a critical issue. An analytical model for the estimate of cruise distance is derived and mobility performance is thus analyzed as a function of cruise speed, relevant vehicle parameters, soil mechanical properties, and atmospheric data. Results are then validated by numerical simulations and an experimental campaign for an Earth-based rover.

1. Introduction

Landed spacecraft can make detailed observations of a planet's surface. However, these observations are restricted to a small area. To obtain coverage over a wider area, spacecraft can carry robots that are able to rove over the surface. Crewed missions or robotic rovers provide not only mobility, but also

[*]Corresponding author
[1]Professor, Department of Engineering for Innovation (DII), giulio.avanzini@unisalento.it
[2]Research Fellow, Department of Industrial Engineering (DIN), emanuele.deangelis4@unibo.it
[3]Associate Professor, Department of Industrial Engineering (DIN), fabrizio.giulietti@unibo.it

the capability to perform complex tasks as well as intelligent and selective observations [1, 2]. For extraterrestrial missions, power is at a premium, and for a planetary rover mission, energy-efficient locomotion is thus critical.

In recent years, a number of missions have been planned and conducted on planets, such as Mars, which involve the use of robotic ground vehicles [3, 4]. Rovers proved their effectiveness and resilience in exploring planets, scouting natural resources, conducting scientific observations, and analyzing samples of the planet soil, in many cases well beyond their intended operational lifetime [5]. Robotic rovers, like Spirit, Opportunity, and Phoenix, which performed exploration of the Martian surface, were all powered by means of rechargeable batteries, using solar power.

When fully illuminated, the rover solar arrays generate about 140 watts of power for up to four hours per sol, provided that the rover needs about 100 watts to drive. The power system for the Mars Exploration Rover includes two rechargeable batteries that provide energy for the rover when the Sun is not shining, during the Martian night. Clearly, an accurate energy balance between energy generated by the panels, stored in the batteries, and used for motion and systems is crucial for maximizing the scientific return of the mission [6].

Similarly, for Moon missions, future vehicles will need to maximize the range covered for a given charge in the battery pack, which is roughly proportional to battery weight. The experience with LRVs on the Moon in the early '70s demonstrated how a guided vehicle can greatly expand the potential of a manned mission to our satellite surface. In the near future, manned mission to the Moon will thus employ mobility systems, based on improved versions

of the Lunar Roving Vehicle (LRV) used by the astronauts of the last three Apollo missions (15, 16, and 17) [7, 8]. Such a development (possibly featuring vehicles of different size and for a wide variety of mission objectives) appears as mandatory, in view of the development of a long-term (or even permanently inhabited) base on the Moon.

In light of this, the objective of this paper is to derive some quantitative guidelines for optimizing vehicle performance within available battery capacity. The data derived can be used by rover designers and scientific mission planners, in order to maximize mission effectiveness. The paper thus provides an analytical framework for investigating performance of electrically-driven ground vehicles powered by battery packs, providing simple indications, useful for preliminary sizing of vehicle battery pack.

Electric vehicles (EVs) have a long history which even precedes the history of gasoline engine vehicles, going back as far as the mid 19th century [9]. However, only in the last decade EVs have received a growing attention. But in spite of the remarkable impulse to study technically feasible solutions for the design of terrestrial EVs, a theoretical evaluation of best range conditions (and corresponding range estimate) for a realistic battery discharge model is not yet available, to the best of the authors' knowledge. This is partially related to the fact that terrestrial vehicles (especially in a short-range city environment) usually undergo wide variations of speed, whereas internal combustion engine are still the only viable solution for long distances [10]. Conversely, extraterrestrial rovers work at an almost constant velocity. An approximately constant power required during the mission thus represents a realistic assumption.

The availability of a sound approach for modeling the power balance between energy stored in the battery packs, power generated by solar panels and power required by rover motors and systems provides a good insight into the relation between rover design parameters and expected performance. A significant improvement in terms of operational capabilities of the vehicle is expected, if a better exploitation of available battery charge allows to cover longer distances.

Some of the main factors influencing terrestrial EV's range are analyzed in [11], with particular focus on environmental conditions, vehicle weight and aerodynamic drag coefficient, driving style during accelerations, and an optimized electric drive, made of properly-sized motors and battery packs. The adoption of range-extending devices [12, 13, 14] and/or battery-switching strategies [15] is typically ruled out from the analysis, because of cost and complexity concerns, for an application to extraterrestrial rovers. Nonetheless, different approaches to enhance performance of battery-only electric vehicles can be found in the literature. Increasing the amount of battery capacity is the simplest way to increase EV range, but this results into a concern on total vehicle mass, provided batteries contribute significantly to the overall EV weight.

Another relevant issue is represented by the need for a reliable estimate of the residual battery charge. Several methods have been developed in order to estimate the state-of-charge of battery packs and the remaining driving range. In Ref. [16], an energy-aware battery management system is proposed to estimate battery voltage as a function of state-of-charge by means of an Extended Kalman Filter. This model-predictive strategy is then used

to modulate the driver control of the vehicle using a setpoint controller for optimizing energy consumption. The sensitivity and reliability of a range estimation algorithm under different operating conditions are evaluated in [17], provided battery voltage is adaptively estimated as in [18], while highlighting that modeling battery behavior is far from trivial, when effective battery capacity depends on temperature, aging, cycling, and current drawn.

The so-called Peukert law adopts a power relationship between discharge current and delivered capacity over some specified range of discharge currents [19]. In Refs. [20] and [21] range equations for electric vehicles are derived using Peukert law for the determination of discharge time as a function of the current drawn, which in turn is obtained from the expression of required power. However, it is important to underline that such analyses based on Peukert law are valid under the hypothesis of constant discharge current at constant battery voltage. These assumptions represent a major simplification of the terms of the problem, provided that battery voltage slowly, yet steadily, decreases during the discharge process and higher currents are thus required to provide the same power to the electric motor [22]. For many applications of interest, a constant-power discharge process is thus more representative of the actual battery loading, as it happens for a steady-speed condition of electric vehicles. In a recent work by the authors [23], where performance of battery-powered aircraft is investigated, an integral formulation for constant-power battery-discharge process is proposed, where time is expressed as a function of discharged capacity and absorbed power.

This paper presents the first application of the empirical battery discharge model recalled above to a class of electrically powered ground vehicles,

namely, extraterrestrial rovers, for which the constant speed/power working condition represents the most likely operational scenario. Note that, for the case of interest, the set of parameters which identify the problem, and in particular, the coefficients in the expression of required power at steady state during the cruise, is different, for example, from that which characterizes the cruise condition for electrically powered fixed-wing aircraft and rotorcraft. Also the effect of environmental conditions (road slope and roughness, type of soil, relative wind, etc.) is different. To this aim, the whole analysis is properly revised to evaluate the set of parameters which identify the optimal cruise condition. As an advantage with respect to existing models for constant-power discharge processes [24], such an integral formulation does not require the knowledge of voltage variations as a function of current and residual capacity.

Starting from the analysis of power required at an approximately constant speed, the constant-power battery discharge model is used to derive a closed-form expression for cruise range, including the effects of different ground scenarios and battery discharge process. Apart from considering the vehicle at steady-state, the solution does not require further simplifying assumptions or numerical discretization related to the use of constant voltage models or models derived from Peukert law. The best range condition is obtained as a function of the parameters which characterize the discharge model, vehicle and soil characteristics and environmental conditions, which significantly affect the optimal cruise condition and its extension [25], as demonstrated in Section 3.

Note that the presence of (possibly strong) winds is a well known feature

of the Martian atmosphere. Moreover, the experimental validation of the EV performance model for a terrestrial rover is performed in the open air, and it is thus subject to the effects of wind. Among other environmental parameters, temperature deserves a comment, provided that it significantly affects battery discharge performance and lifetime [26]. Rechargeable batteries can age prematurely at high temperatures (above 40°C) and electrolytes can freeze at low temperatures (below -30°C). In order to keep battery temperature between safe limits and reduce the magnitude of temperature cycles (as it occurs during Martian diurnal cycles) [27], different passive or active thermal control techniques have been considered. Provided the electronics temperature is maintained between safe limits, the estimation of the cruise range and the identification of the optimal driving strategy can be fine tuned according to scheduled set of battery discharge model parameters (previously characterized on Earth through laboratory tests at different operating temperatures).

The availability of an analytical solution for the evaluation of vehicle range is particularly beneficial for preliminary design of EVs, where the optimal relation between vehicle empty weight, payload, and weight of battery pack (proportional to capacity) is readily available and allows for a quick evaluation of the effect of different vehicle configurations. Moreover, the optimal speed which maximizes the range can be obtained by means of simple and efficient numerical algorithms, such as Newthon-Raphson scheme [28], parabolic search or simplex method [29]. It should be also underlined that dynamic terms (e.g. power required for accelerating the vehicle) could be easily included in the analysis, if necessary. As an example, if a set of repeti-

tive tasks is envisaged for the EV, it is possible to identify a discharge model that iterates the energy loss for each cycle, thus deriving a mission-specific optimal condition basically using the same set of tools and the same battery discharge model.

In the next section, the power balance of the EV and the battery discharge model are discussed in the most general case. The analytical derivation of the range equation and the determination of the optimal, maximum range, travel condition is the subject of Section 3. In Section 4 numerical and experimental results are analyzed. First, a comparison with a Peukert-based discharge model is considered for a numerical test-case applicable to a terrestrial vehicle. An experimental campaign, performed on a small-scale monster truck at the University of Bologna premises, shows the effectiveness of the proposed technique and outlines a procedure with general validity for range optimization of any electrically-driven vehicle and different battery technologies. The approach is finally validated by numerical simulations for a relevant Lunar environment [30], where comparisons with actual data for the LRV used during the last Apollo missions are performed. A section of concluding remarks ends the paper.

2. System Modeling

2.1. Analysis of Required Power

The total power required by a vehicle moving up a grade in a steady speed condition is

$$P_{req} = P_{aux} + P_{st} + P_{mot} \tag{1}$$

where P_{aux} is the power required for on board auxiliary systems and possible power-consuming payload (assumed to be independent from forward speed

U), P_{st} is the power necessary to steer the vehicle, and $P_{mot} = F_{mot}\,U$ is the power necessary to overcome the resistance, F_{mot}, along the vehicle direction of motion (see Fig. 1).

It is supposed that steering capabilities are provided by an Electric Power Steering (EPS) system made of a number N_{st} of operative front and/or rear electric actuators. The power required from the EPS strongly depends on the particular trajectory followed and the presence of obstacles to avoid (wander factor contribution), soil condition, and vehicle speed. In particular, for increasing vehicle speed, steering activity should be gradually moderated to ensure proper maneuvering stability at high speed. According to the results obtained in [31] for a vehicle in motion, the power necessary to steer can be approximated as a linear function of vehicle speed, namely

$$P_{st} = P_{st0} + P_{st1}\,U \tag{2}$$

where $P_{st0} > 0$ and $P_{st1} \leq 0$, provided P_{st} remains non-negative over the considered speed range. In the case of a manned vehicle, such parameters are determined experimentally and are strongly related to the pilot's driving style. When an unmanned rover is analyzed, P_{st0} and P_{st1} are typically designed in order to satisfy a prescribed set of requirements posed on the trajectory tracking performance and stability.

The total motion resistance F_{mot} is given by the following contributions:

$$F_{mot} = F_d + F_r + F_g + F_s \tag{3}$$

where F_d is aerodynamic drag, F_r is the rolling resistance determined by N wheels on the considered surface, F_g is the grade resistance, and F_s is the

equivalent motion resistance obtained by taking into account power losses in the vehicle suspension system.

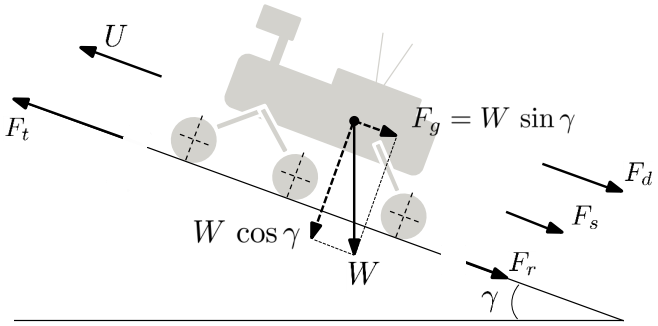

Figure 1: Forces acting along vehicle moving direction.

Aerodynamic drag is expressed as [32]

$$F_d = 0.5\,\rho\,A\,C_D\ (U + U_w)^2 \tag{4}$$

where ρ is density of the atmosphere, A is vehicle frontal area, and C_D is the aerodynamic drag coefficient. U_w is the component of wind speed (assumed to be a constant) along the vehicle moving direction, which has a positive sign when this component is opposite to the vehicle speed and a negative sign when it is in the same direction as the vehicle speed.

The rolling resistance on soft surfaces, given by:

$$F_r = F_r^{(ext)} + F_r^{(int)}, \tag{5}$$

consists of two major components: the internal losses in the wheel or track, determined by bearing friction and wheel deflection, represented by the resistance $F_r^{(int)}$, and the external force $F_r^{(ext)}$, expended on deforming the soil. There are several other losses: the bulldozing of soil in front of the tread, and the drag losses along the sides of the tread. These are usually low values

and are neglected in this framework. The internal losses can be calculated by considering the rolling resistance of a flexible wheel on a hard surface [30], namely:

$$F_r^{(int)} = \mu W \cos\gamma \tag{6}$$

where W is vehicle weight, γ is the surface slope angle, and μ is the rolling resistance coefficient, which depends on surface and wheel condition and vehicle speed. Based on experimental results, many empirical models can be found in the literature for calculating the rolling resistance coefficient on a hard surface. For the purposes of the present paper, μ is assumed to be a linear function of speed [32], namely

$$\mu = \mu_0 + \mu_1 U \tag{7}$$

where μ_0 and μ_1 are positive coefficients to be determined experimentally. The external resistance is based on the soil-vehicle model referred to by Rula and Nuttal [33] as the "Bekker/LLD soil-vehicle model C_w," which is mainly applicable to wheels with flexible tires interacting with soft soil. In particular, the external resistance increases as the vehicle sinks into the soil. Wheel sinkage (in) is calculated as

$$z = \left(\frac{W\cos\gamma}{NSk}\right)^{\frac{1}{m}} \tag{8}$$

where W must be expressed in lb, S is wheel footprint area (in^2), m is a dimensionless exponent of soil deformation, and $k = k_c/d + k_\phi$ is soil consistency coefficient (lb/in^{m+2}), provided k_c is cohesive modulus of soil deformation (lb/in^{m+1}), d is tire width of ground contact (in), and k_ϕ is frictional modulus of soil deformation (lb/in^{m+2}). The total external resistance (N)

caused by soil compaction is equal to

$$F_r^{(ext)} = N\,\xi\left(\frac{d\,k}{m+1}\right) z^{m+1} \tag{9}$$

where $xi = 4.448222$ N/lb is a conversion factor from pounds to Newton.

The grading resistance is represented by the component of vehicle weight along the moving direction:

$$F_g = W\,\sin\gamma \tag{10}$$

The total damper power losses are computed from the relation $P_s = N\,k_r\,U^2$, where $k_r = \bar{k}_r/3\,317.76$, provided $3\,317.76$ is a conversion factor and $\bar{k}_r$ is the (dimensionless) surface roughness coefficient. Based on power spectral density estimates obtained from geological analysis, $\bar{k}_r$ takes into account the irregularities of the soil surface caused by factors such as soil texture, aggregate size, and rock fragments. It is quantified by the deviations in the direction of the normal vector of the real ground surface from its smooth ideal form. For the aim of the present analysis, an equivalent resistance is evaluated as $F_s = P_s/U$, namely:

$$F_s = N\,k_r\,U \tag{11}$$

Given Eqs. (4)-(11), the total resistance in Eq. (3) becomes:

$$F_{mot} = f_2\,U^2 + f_1\,U + f_0 \tag{12}$$

where

$$\begin{aligned} f_0 = {} & 0.5\,\rho\,A\,C_D\,U_w^2 + W\,(\sin\gamma + \mu_0\,\cos\gamma) \\ & + N\,\xi\left(\frac{d\,k}{m+1}\right) z^{m+1} \end{aligned} \tag{13}$$

$$f_1 = \rho\, A\, C_D\, U_w + \mu_1\, W\, \cos\gamma + N\, k_r, \tag{14}$$

and

$$f_2 = 0.5\, \rho\, A\, C_D \tag{15}$$

2.2. Analysis of Available Power

Consider the sketch in Fig. 2, where a simplified electrical system is outlined for a sample rover. The power output of the battery pack(s) is processed by the Power Management Unit (PMU), which includes all regulation systems that allow safe distribution of available power to vehicle users, according to the required standards [34]. Note that the battery power is reduced by losses within the PMU internal circuitry, made of transformers, converters, voltage stabilization systems, and load control devices. For the aim of the present study, an overall constant efficiency η_{pmu} is assumed to characterize the PMU task, provided that more accurate analyses are typically made available at an advanced rover design stage.

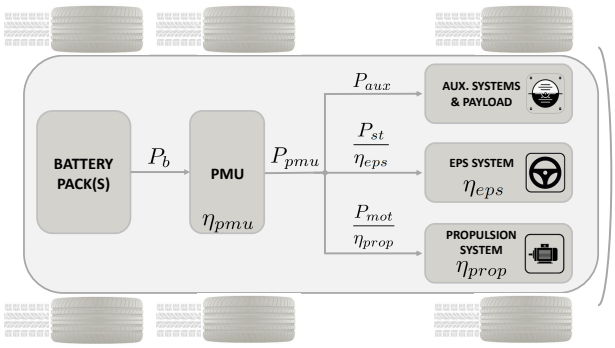

Figure 2: Power distribution system of a sample rover.

The power output P_{pmu} of the PMU is delivered to the electric users through dedicated buses. According to Eq. (1) and Fig. 2, a certain amount of power, P_{aux}, is absorbed by auxiliary systems and payload, while the

power dedicated to the EPS system is reduced by losses, accounted for by the efficiency η_{eps}, within the steering actuators and the electric regulators. Finally, let F_t be the tractive effort produced by the powerplant torque and transferred through transmission and final drive to the drive wheels. In a steady-speed condition, the power required to overcome the total resistance, P_{mot}, and the available tractive power, $P_t = F_t\,U$, are equal (assuming no wheel slip). As a matter of fact, the power delivered to the propulsion system is reduced by losses within the electric powertrain system made of speed regulators, single or multiple electric motors, the transmission system, and the final drives. Although each subsystem has its own efficiency, η_r, η_m, η_t, and η_d respectively, for the purpose of the present work, they are combined into an overall propulsive efficiency, $\eta_{prop} = \eta_r\,\eta_m\,\eta_t\,\eta_d$. When no multi-speed transmission is present in the drivetrain, the overall efficiency can be considered as a function of vehicle speed only, $\eta_{prop} = \eta_{prop}\,(U)$.

Taking into account Fig. 2 and imposing the balance between required and available power, it follows that

$$P_{pmu} = \frac{P_{mot}}{\eta_{prop}} + \frac{P_{st}}{\eta_{eps}} + P_{aux} \tag{16}$$

Provided $P_b = P_{pmu}/\eta_{pmu}$ is the battery output power, one has

$$P_b = \frac{1}{\eta_{pmu}} \left(\frac{P_{mot}}{\eta_{prop}} + \frac{P_{st}}{\eta_{eps}} + P_{aux} \right) \tag{17}$$

where the terms P_{st} and P_{mot} can be expressed according to Eqs. (2) and (12)-(15), respectively. Provided η_{prop} is positive over the considered speed range, one has that

$$\begin{aligned} P_b &= \frac{1}{\eta_{pmu}} \left[\frac{F_{mot}\,U}{\eta_{prop}\,(U)} + \frac{P_{st0} + P_{st1}\,U}{\eta_{eps}} + P_{aux} \right] \\ &= p_3(U)\,U^3 + p_2(U)\,U^2 + p_1(U)\,U + p_0 \end{aligned} \tag{18}$$

where

$$p_0 = \frac{P_{st0} + \eta_{eps}\, P_{aux}}{\eta_{pmu}\, \eta_{eps}} \tag{19}$$

is constant, whereas

$$p_1\,(U) = \frac{f_0\, \eta_{eps} + P_{st1}\, \eta_{prop}\,(U)}{\eta_{pmu}\, \eta_{eps}\, \eta_{prop}\,(U)} \tag{20}$$

$$p_2\,(U) = \frac{f_1}{\eta_{pmu}\, \eta_{prop}\,(U)} \tag{21}$$

$$p_3\,(U) = \frac{f_2}{\eta_{pmu}\, \eta_{prop}\,(U)} \tag{22}$$

depend on vehicle speed. Please, note that in the presence of solar arrays, the required power is reduced by the amount of solar energy generated by the panels per unit time. This can be seen as a negative contribution to the total required power, which recharges the battery when it exceeds the power required for motion and systems.

3. Vehicle Performance

3.1. Maximum range for a constant power discharge process

Consider the expression obtained in Eq. (18). It can be noted that, for a vehicle in a steady speed condition, the battery power is a constant. In Ref. [23] a novel formulation for constant-power battery discharge process is proposed, where discharge time is expressed as a function of discharged capacity and absorbed power. Let $I = I(t)$ be the current provided by the battery pack at time t and $C = C(t)$ be the discharged capacity, obtained as

$$C(t) = \int_0^t I(s)\, ds \tag{23}$$

Assuming $P_b > 0$, the discharge process is stopped at time t_f, when $C_f = C(t_f) = K\, C_0$, with C_0 equal to the nominal battery capacity and $K < 1$

a predefined discharge percentage. Discharge time can be expressed in the form

$$t_f = \delta \, P_b^{\epsilon} \, C_f^{\beta} \tag{24}$$

where coefficients $\delta > 0$, $\epsilon < -1$, and $0 < \beta < 1$, which depend on battery technology, ambient temperature, and number of series-connected cells, are determined experimentally. Provided $x = t_f \, U$ is cruise range, from Eqs. (18) and (24) one gets:

$$x = \delta \, P_b^{\epsilon} \, C_f^{\beta} \, U \tag{25}$$

Taking into account Eq. (18), the latter equation becomes

$$\begin{aligned} x = \delta \, \big[& p_3(U) \, U^3 + p_2(U) \, U^2 \\ & + p_1(U) \, U + p_0 \big]^{\epsilon} \, C_f^{\beta} \, U \end{aligned} \tag{26}$$

A necessary condition for the optimal value of U which maximizes the distance x, that is, the best range speed, $U = U_{br}$, is obtained by solving the equation $dx/dU = 0$. The sign of the first derivative before and after its zeros (or, equivalently, the sign of the second derivative at the zeros) allows for identifying maxima and minima of the range curve. In the most general case η_{prop}, which is typically estimated from vehicle datasheet or determined experimentally, may depend on speed U. Hence, an analytical solution for the equation $dx/dU = 0$ and the sign of d^2x/dU^2 with general validity is not available. An iterative root search algorithm, such as Newton-Raphson scheme [28], needs to be implemented and the second derivative at the zero can be evaluated by means of centered differences. As an alternative, the function that relates vehicle speed to the expected range performance in Eq. (26) can be plotted and the best range condition identified either graph-

ically on the plot or numerically by means of a search algorithm, such as the parabolic search or the simplex method [29].

When η_{prop} is constant, the expression of dx/dU is proportional to a third order polynomial, and $dx/dU = 0$ if

$$(3\epsilon + 1)p_3\,U^3 + (2\epsilon + 1)p_2\,U^2 + (\epsilon + 1)p_1\,U + p_0 = 0 \tag{27}$$

which has, in general, only one real positive solution, for realistic values of system parameters. For example, when no wind nor slope is present along an ideal straight trajectory, all the coefficients of the terms in Eq. (27) with a U power are negative, and only the last one, namely the term related to P_{aux} and P_{st0}, is positive. The sequence of signs is thus $---+$, which indicates that, according to Descartes' rule, there is only one real positive solution [35]. When there is a slope, only the linear term in U, namely $(\epsilon+1)p_1$, may change sign, with the sequence becoming $--++$. Again, this represents a sufficient condition for proving that there is only one real positive root of the polynomial, in the form:

$$U_{br} = -\frac{1}{3(3\epsilon + 1)\,p_3}\left[(2\epsilon + 1)\,p_2 + Q + \frac{R}{Q}\right] \tag{28}$$

where

$$\begin{aligned} Q &= \sqrt[3]{\frac{S + \sqrt{S^2 - 4\,R^3}}{2}} \\ R &= (2\epsilon + 1)^2\,p_2^2 - 3(3\epsilon + 1)(\epsilon + 1)\,p_1\,p_3 \\ S &= 2(2\epsilon + 1)^3\,p_2^3 + 27(3\epsilon + 1)^2\,p_3^2\,p_0 \\ &\quad - 9(3\epsilon + 1)(2\epsilon + 1)(\epsilon + 1)\,p_1\,p_2\,p_3 \end{aligned} \tag{29}$$

Provided that the polynomial in Eq. (27) grows towards $-\infty$ as $U \to +\infty$, the first derivative is expected to be positive before the root and negative

after it, thus indicating that the zero of the first derivative corresponds to a maximum for x.

Only when slope and wind forces combine in terms with opposite directions, a more complex situation with two maxima and one local minimum for x can be found, which, by the way, is obtained for unusually high values of slope angle and/or wind. Thus, in the most realistic cases, the positive real root is the only real solution of the polynomial equation, which can be easily determined by means of a root-finding numerical algorithm or Cardan formulas [28].

3.2. Vehicle range for variable power

The analytical solution in Eq. (27) for the approximate model with constant η_{prop}, or the numerical one for a more realistic model, which accounts for variations of overall powertrain efficiency with working conditions, both provide a best range speed under the assumption of constant power during the whole cruise. The results obtained within this framework can be useful for preliminary sizing of a vehicle, accounting for an average power drawn from the batteries during a reference mission. However, mission planning typically requires to account for possible variations of the environment (soil, slope, prevalent wind, etc.), which makes the constant power assumption unrealistic. In order to develop a more general mission planning tool, which can account for variations of power required during different mission segments, a variable power battery discharge model is also introduced.

Assume that the battery is discharged at power P_b for a time interval $t_d < t_f$. A residual discharge time $t_r = t_f - t_d$ at power P_b is thus available, which can be related to a corresponding value of a residual battery charge,

C_r, where $t_r = \delta\, P_b^{\epsilon}\, C_r^{\beta}$, which implies

$$C_r = [(t_f - t_d)/(\delta P_b^{\epsilon})]^{1/\beta}$$

The available residual discharge time, $\hat{t}_r$, for a different value of the power drawn from the battery, $\hat{P}_b$, can be estimated as $\hat{t}_r = \delta\, \hat{P}_b^{\epsilon}\, C_r^{\beta}$, and the process can then be iterated for a second segment, if its duration is less than $\hat{t}_r$.

Letting C_k be the residual charge available at the end of the k-th mission segment, which requires an average power P_{bk} and lasts Δt_k, it is

$$C_k = [C_{k-1}^{\beta} - \Delta t_k/(\delta P_{bk}^{\epsilon})]^{1/\beta}$$

The rover mission, made of N segments which require different average power, P_{bk}, $k = 1, 2, \ldots, N$, because of soil and/or slope variations, is thus feasible if the residual charge at the end of the last segment is non-negative, that is $C_N > 0$. Moreover, the best range speed evaluated in Section 3.1 also provides the speed which minimizes the charge drawn from the battery for a given distance, thus maximizing the residual charge at the end of the segment.

If one needs to maximize mission effectiveness (e.g. by maximizing the residual charge at the end of the mission, so that a shorter time is required for the recharge process), each segment needs to be performed at the best range speed for the required power level. The determination of the best range speed, if compatible with mission objectives, thus provides a precious tool for rover mission analysis and design. If vehicle velocity is constrained by other factors, it is still possible to determine the maximum distance that can be covered over a portion of the planet surface where condition can vary.

4. Results

The approach presented in Sections 2 and 3 is validated for three test cases. First, the results of numerical simulations and an experimental campaign are reported for sample terrestrial rovers. In particular, the effect of different wind conditions and road slopes is investigated in the simulation scenario. The best range speed is then derived following the approach outlined in Section 3. The analysis of required power is finally reported for the LRV, based on actual data from the last three Apollo missions. Vehicle performance is investigated and numerical results are then compared to those available from the Extra Vehicular Activity (EVA) reports. In what follows, measurement units are expressed in the metric system, except where otherwise indicated.

4.1. Terrestrial Rover: Simulation Results

Consider a small-scale four-wheeled rover characterized by $W = 30$ N, powered by a 3S Li-Po battery pack with nominal voltage $V_0 = 11.1$ V and nominal capacity $C_0 = 2.2$ Ah. The parameters for the aerodynamic drag model are $\rho = 1.225$ kg m^{-3}, $A = 0.06$ m^2, and $C_D = 0.25$. The vehicle moves along an ideal straight line on dry smooth asphalt, such that no steering is required ($P_{st} \approx 0$ W), power losses in the vehicle suspension system are negligible ($k_r \approx 0$), and the rolling resistance is only determined by tire internal losses, according to Eq. (6) (namely, wheel sinkage $z \approx 0$ m). The coefficients for the rolling resistance of the vehicle are $\mu_0 = 0.01$ and $\mu_1 = 3.6 \cdot 10^{-4}$ s/m [32]. The power required for on board auxiliary systems and payload is $P_{aux} = 11.3$ W, the PMU is characterized by $\eta_{pmu} = 0.94$,

and the efficiency of the propulsion system is assumed to be a constant, $\eta_{prop} = 0.85$.

The battery model coefficients in Eq. (24) were estimated from a dedicated test campaign performed according to the procedure described in [23] on a FullPower® battery pack at the ambient temperature $T_0 = 26°C$, using a Maynuo® M9715 DC electronic load, which allows discharge programs at constant power. Expressing discharge time t in hours, the battery model parameters are $\delta = 12.23$, $\epsilon = -1.014$, and $\beta = 0.9644$.

Numerical simulations are performed for different wind and slope conditions. The following scenarios are presented and discussed: 1) the vehicle moves downhill in the presence of a tailwind component; 2) the vehicle moves on level dry asphalt in quiet air; 3) the vehicle moves uphill in the presence of a headwind component. The parameters adopted for the three cases and the values of motion resistance coefficients in Eqs. (14) and (15) are reported in Table 1.

Table 1: Numerical analysis (terrestrial rover): total resistance parameters.

Case	γ [deg]	U_w [m/s]	f_2 [N/(m/s)^2]	f_1 [N/(m/s)]	f_0 [N]
1	-2	-1	0.0092	-0.0076	-0.7380
2	0	0	0.0092	0.0108	0.3
3	+2	+1	0.0092	0.0292	1.3560

The total power required from the battery in a steady speed condition is plotted in Fig. 3.b as a function of ground speed. The corresponding range, calculated according to Eq. (18) for a 80% usage of battery nominal capacity, is reported in Fig. 3.a, where the best range condition (in what follows indicated with the subscript 'br') is highlighted by means of a $\times$

symbol for each one of the considered cases. Maxima were determined by applying a Newton-Raphson method to Eq. (27). The algorithm converges in 3 or 4 iterations, using the midpoint for the considered speed range as initial guess and requiring a residual error below 10^{-4} m/s at convergence. Results are summarized in Table 2.

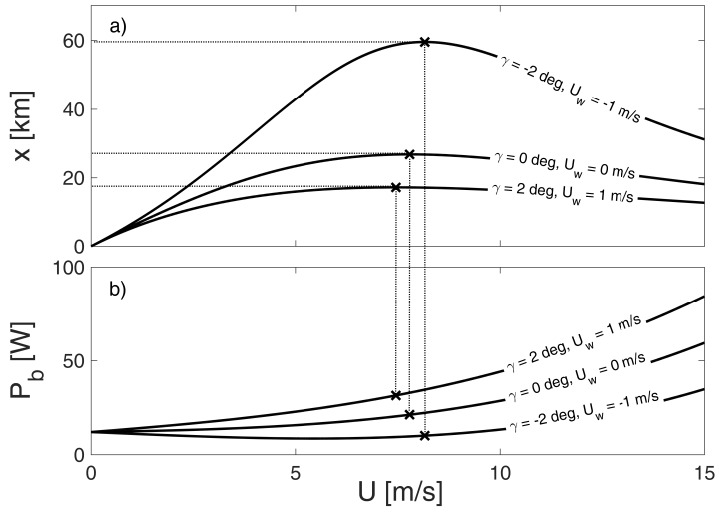

Figure 3: Numerical analysis (terrestrial rover): power and range as a function of cruise speed.

Table 2: Numerical analysis (terrestrial rover): best range conditions.

Case	γ [deg]	U_w [m/s]	U_{br} [m/s]	P_{bbr} [W]	x_{br} [km]
1	-2	-1	8.2	10.09	59.51
2	0	0	7.8	21.19	26.78
3	+2	+1	7.5	31.45	17.17

Note from Table 2 that the best range speed becomes smaller when the driving scenario determines a more demanding power profile and the achievable range decreases. However, the variation of the optimal speed is relatively small, if one considers that a reduction of only -8.6% occurs in U_{br} going

from Case 1 to Case 3, compared to a corresponding reduction of the achievable best range as large as -71.2%, due to an increase in the required power almost by a factor 3. Also, the maximum in the range curves becomes 'flat' if a less favorable scenario is considered, resulting into a more acceptable degradation of performance if a deviation from the best range speed occurs. In Case 1, for example, a 10% decrease of speed from the optimal value results into -1.9% of range degradation. In Case 3, the same percentage deviation from the best range speed determines a variation as small as -0.58% with respect to the maximum range. It is worth noting that, unlike Cases 1 and 2, the power curve of Case 3 is not monotonically increasing over the considered range of speed, showing, in particular, a minimum for $U = U_{P_{bmin}} = 5.5$ m/s. According to the battery model in Eq. (24), such a minimum-power condition allows the vehicle in the considered scenario to perform maximum endurance for a value of speed different than zero.

In Fig. 4 vehicle range estimation performed by Eq. (26) is further discussed and validated by experimental data. Starting from the analytical results obtained for Case 2, summarized in the second line of Table 2, an experiment is performed where the FullPower® battery pack is discharged by means of the electrical load to the 80% of the nominal capacity C_0, at the constant power $P_b = P_b\,(U_{br}) = 21.19$ W. In such a case, discharge time results to be $t_{exp} = 57.2$ min, corresponding to the range $x_{exp} = t_{exp}\,U_{br} = 26.77$ km. The estimation error between the model-predicted range at $U = U_{br}$ and the corresponding one obtained experimentally is 0.04%. A comparison is also performed for other two values of vehicle speed, calculated as $0.5\,U_{br}$ and $1.5\,U_{br}$, where the required battery power is given by 14.33 W and 36.59 W,

respectively. The estimation errors with respect to the experimental values respectively result into -0.05% and -0.35%, thus showing the effectiveness of the proposed approach (see the circle markers in Fig. 4).

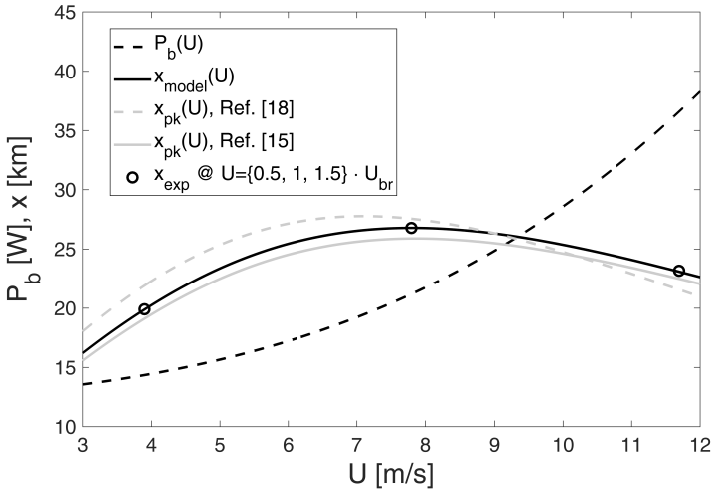

Figure 4: Numerical analysis (terrestrial rover): range as a function of cruise speed for different battery-discharge models (Case 2).

A comparison to a classical Peukert-based approach is also provided for Case 2, where the assumption of constant current during battery discharge is considered. In the present framework, the equivalent constant voltage is considered as the mean value between the open-loop fully charged battery voltage and the nominal voltage, namely $V_e = (V_f + V_0)/2 = 11.85$ V, provided $V_f = 12.6$ V. Hence, the equivalent constant current relative to the discharge at P_b =const. is $I_{pk} = P_b/V_e$. Let R_t be the battery hour rating, that is the discharge time over which the nominal capacity was determined by the manufacturer (typically 1 h for small rechargeable battery packs). Provided $n = 1.19$ is the Peukert coefficient estimated for the considered battery at $T_0 = 26°$C, predicted endurance is given by Peukert equation

$t_{pk} = R_t^{1-n} (K\, C_0\, V_e / P_b)^n$ (where $K = 0.8$), according to the formulation used in [23]. In the case when $n = 1$, the ideal situation in which discharge time is simply inversely proportional to the absorbed power is obtained according to [20], provided the equivalent constant voltage is assumed to be equal to the nominal voltage, namely $V_e = V_0$, and $C_0 V_0 = 24.42$ Wh is the battery nominal energy.

The variation of range with speed obtained for the battery model derived for a constant power discharge process (solid black line in Fig. 4) is compared to the range evaluated for the classic Peukert (constant current) discharge process described above (dashed gray line in the same figure) and the ideal battery model (solid gray line). The ideal battery model provides a slightly shorter range estimate at all considered velocities, with a difference in the order of 3%. Conversely, Peukert's law provides a higher estimate at slower speed, with an increase in range estimate as high as almost 10%, in the lower speed range, where current drawn from the battery is smaller, thus determining a beneficial effect on effective battery capacity for a Peukert exponent $n > 1$. The difference with respect to the constant power discharge model vanishes, for the considered test case, at approximately $U = 9$ m/s, where higher currents are drawn from the battery and Peukert's effect determines a reduced effective battery capacity.

Fig. 4 also shows that maximum range is attained by the three battery models at different speeds. The best range condition obtained by means of the two Peukert-based formulations described above are summarized in Table 3. These results can be compared with those reported, for the same operational conditions, on the second line of Table 2). Once again, the differ-

ence is less significant for the ideal battery, which provides an almost identical value of the best range speed, if compared to that obtained for the constant power discharge model. Also note that, if the value reported in the first line of Table 3 was assumed as the best range speed, where $P_b = 19.45$ W, the range calculated by the model in Eq. (26) would provide a sub-optimal condition, where $x = 26.59$ km, with a variation which is only 0.71% smaller than the value reported in Table 2. Conversely, the use of Peukert's law provides a significantly lower best range speed, although also in this case the actual range evaluated by means of the constant power discharge model would be reduced by approximately 1% only.

Table 3: Numerical analysis (terrestrial rover): vehicle best range conditions according to Peukert-based approaches (Case 2).

Peukert model	n	V_e [V]	U_{br} [m/s]	P_{bbr} [W]	x_{br} [km]
Ref. [23]	1.19	11.85	7.1	19.45	27.77
Ref. [20]	1	11.1	7.9	21.37	25.88

As a final example, the variable power battery discharge model is applied to a case where the rover is assumed to drive along an 8 km long level pattern, followed by a climb (2 km at 10 deg of slope, then 1 km at 30 deg), reaching a plateau, almost 850 m higher than the initial altitude, where a scientific payload is activated. The payload requires 10 W of power, which, during this last phase, adds to the rover system power (12 W). As reported in Tab. 4, three missions performed at constant speed, equal to 4, 8, and 12 m/s, respectively, are considered, together with a fourth, optimal one, where the best range speed is considered for each mission segment, depending on the required power. In this case, the optimal speed is 7.8 m/s during

the initial segment, 7.6 and 7.4 m/s during the two climb segments, respectively, and 9.6 m/s when the payload is activated along the level pattern on the plateau. Acceleration and deceleration transients between segments have a negligible impact on the overall energy balance of the mission and are thus neglected. Table 4 shows that the residual charge at the end of the

Table 4: Numerical analysis (terrestrial rover): performance analysis of a sample four-segment mission.

speed [m/s]	res. capacity at the end of $k-$th segment [Ah] $K\,C_0$	C_1	C_2	C_3	residual range [km]
4	1.76	1.088	0.616	0.088	0.66
8	1.76	1.256	0.824	0.314	3.46
12	1.76	1.161	0.703	0.178	1.96
U_{brk}	1.76 (7.8 m/s)	1.257 (7.6 m/s)	0.825 (7.4 m/s)	0.315 (9.6 m/s)	3.56

climb varies significantly, as a function of the speed of the rover during the approach and climb, thus resulting in large difference in the available range for performing the mission, with the payload switched on. At the same time, the total distance covered on the plateau for a constant speed of 8 m/s is only marginally shorter than the longest possible pattern, obtained when all mission segments are performed at the best range speed. This is due to the fact that the maxima of the range curves are flat, becoming flatter as the power drawn from the batteries gets higher. Hence, rover cruise performance does not vary significantly, if rover speed remains sufficiently close to the best range value. As an interesting consequence of this result, the assumption of an average power during the whole mission provides a reliable global performance index, in terms of overall distance, without the need of

a detailed analysis of the power drawn during each mission segment and the determination of the corresponding optimal speed.

Remark 1 Note that guidelines for preliminary sizing of vehicle battery can be derived from Eqs. (19)-(22), (24), and (25). As an example, a procedure similar to the sizing approach proposed in Ref. [23] for fixed-wing electric aircraft can be obtained. After expressing vehicle weight as $W = W_0 + W_b$, where W_0 is the operative empty weight (that includes structure, propulsion system, payload, and auxiliary systems weight) and W_b is battery weight, let $\sigma = W_b/E_0 = W_b/\left(V_0\, C_0\right)$ indicate battery weight/energy ratio (that is, the inverse of battery energy density) and assume that the discharge process is stopped at time t_f, when $C_f = C(t_f) = K\, C_0$. Vehicle total weight is now written as $W = W_0 + \sigma\, V_0\, C_0$ such that, for a desired endurance or range, Eqs. (24) and (25) are, respectively, a function of the only variable C_0. For a desired speed U, the latter equations can be solved in terms of C_0 by a numerical algorithm, such as Newton's iterative scheme [28], thus providing the design nominal capacity required for the considered vehicle performance. For the terrestrial rover analyzed in Case 2, with $W_0 = 28.14$ N and $\sigma = 0.0763$ N/(Wh), assuming $C_0 = 2.2$ Ah, it follows $W_b = \sigma\, V_0\, C_0 = 1.86$ N and $W = W_0 + W_b = 30$ N, as already pointed out. Suppose the vehicle is designed to perform a mission at constant speed $U = 10$ m/s. With the given battery, endurance and range respectively result to be $t = 42.3$ min and $x = 25.25$ km with $K = 0.8$. If desired endurance is set as $t_d = 70$ min, the required nominal capacity becomes $C_0 = 3.75$ Ah, while $W_b = 3.17$ N and $W = 31.31$ N. On the other hand, if a requirement is set on the desired range, for example $x_d = 60$ km, the required nominal capacity becomes

$C_0 = 5.47$ Ah, while $W_b = 4.63$ N and $W = 32.77$ N.

4.2. Terrestrial Rover: Experimental Results

The terrestrial vehicle considered for the test campaign is a Traxxas® E-Maxx, depicted in Fig. 5, a small-scale monster truck with a weight $W = 47.88$ N and a wheelbase $l = 0.34$ m. Traction is provided by a four-wheel drive powered by two Titan® fan-cooled 14.4 V 550-size motors through a Cardan shaft. Motor regulation is performed by a 14.4 V EVX-2® Electronic Speed Controller which is operated by a Ardupilot® Mega (APM) 2.6. The main board is connected with a 3DR® GPS uBlox LEA-6 with Compass module and a 3DR® 433 MHz telemetry module. Remote control commands are processed by a 2.4 GHz FrSky TFR8 onboard receiver. Vehicle motors and on board systems are powered by a 4S Li-Po battery pack by Turnigy®, with a nominal voltage $V_0 = 14.8$ V and a nominal capacity $C_0 = 5.4$ Ah. Battery model coefficients, estimated by a dedicated test campaign at ambient temperature $T_0 = 26°$C, are $\delta = 18.54$, $\epsilon = -1.026$, and $\beta = 0.9670$.

The first phase of the experimental campaign is represented by the identification of the curve describing required battery power as a function of speed, without prior knowledge of system parameters that characterize p_0, $p_1(U)$, $p_2(U)$, and $p_3(U)$ in Eqs. (19)-(22). To this aim, the vehicle was driven along a straight line on level dry asphalt, $\gamma = 0$ deg, at different constant throttle settings, in the absence of wind components, $U_w = 0$ m/s. The vehicle speed and the corresponding power consumption, respectively calculated from GPS and a wattmeter sensor, were obtained as the mean value over $\Delta t = 5$ s for each driving segment at constant throttle setting (note that

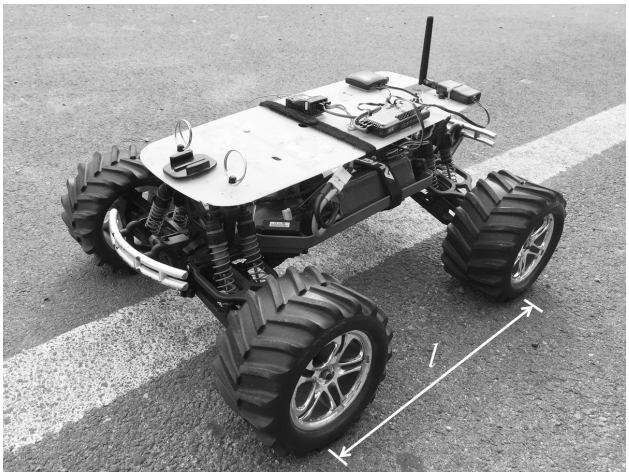

Figure 5: Battery-powered RC car used for the experimental campaign.

Δt was selected in order to exclude the vehicle acceleration phases). The results are summarized in Table 5, where the first line reports battery power at rest, namely $P_b\,(U = 0) \approx P_{aux}/\eta_{pmu}$, directly measured by laboratory test. Experimental data in terms of battery power consumption are provided

Table 5: Experimental results (terrestrial rover): power consumption as a function of speed.

segment	throttle [%]	speed [m/s]		battery power [W]	
		mean	std. dev.	mean	std. dev.
1	0	0	-	2.2	-
2	10	1.6	0.09	17.08	2.70
3	20	3.9	0.09	42.05	0.43
4	30	6.3	0.26	74.16	0.76

in Fig. 6 (see the circle markers). Note that an ad-hoc characterization of efficiency η_{pmu}, η_{eps}, and $\eta_{prop} = \eta_{prop}(U)$, as described in Eq. (18), is not necessary in this framework. In fact, according to the experimental setup, the wattmeter directly estimates electrical power required from the battery

pack as $P_b = V\,I$, where V is battery voltage, thus including any mechanical and electrical loss which occurs between the battery pack and the wheels. In the present case, the function in Eq. (18) is approximated by a polynomial with constant coefficients, based on experimental data. In particular, a third order polynomial is used for curve fitting, according to Eq. (18), such that $P_b\,(U) = p_3\,U^3 + p_2\,U^2 + p_1\,U + p_0$, where $p_3 = 0.0635$ W/(m/s)^3, $p_2 = -0.03163$ W/(m/s)^2, $p_1 = 9.24$ W/(m/s), and $p_0 = P_s = 2.2$ W (see the dot line in Fig. 6). Estimated range as given by Eq. (25) is also reported for $K = 0.8$ (solid line in Fig. 6). The best range speed results to be $U_{br} = 2.4$ m/s, where $P_{bbr} = 25.05$ W and $x_{br} = 24.21$ km.

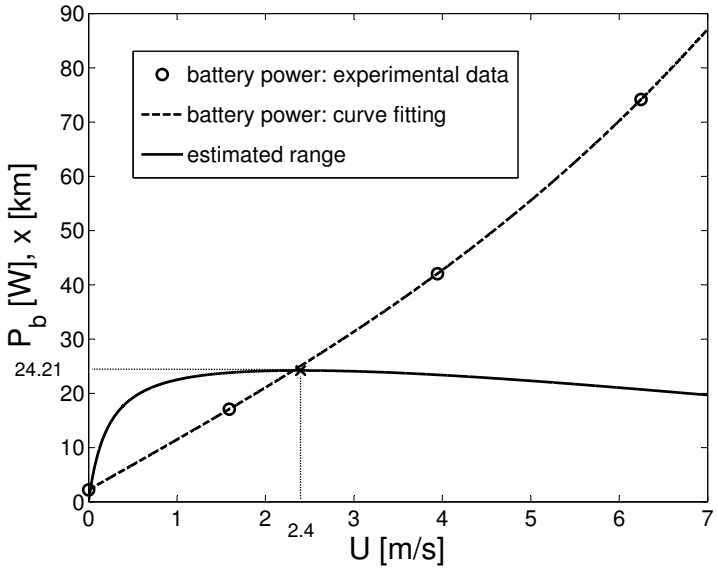

Figure 6: Experimental results (terrestrial rover): battery power consumption as a function of speed.

In order to prove the effectiveness of the proposed approach, data collected during the experimental campaign are also used to identify, for each i-th constant-speed segment, the reference quantity $x_k/\Delta C_k$, $k = 1, \ldots, 4$,

where x_k and ΔC_k are, respectively, the range and the capacity discharged during the i-th segment at the constant speed U_k (calculated as the mean value over $\Delta t = 5$ s reported in Table 5). Note, in particular, that $x_1/\Delta C_1 = 0$ km/(Ah) since no range is covered at $U_1 = 0$ m/s, while a certain amount of discharged capacity, $\Delta C_1 \neq 0$ Ah, is used to power systems. With regard to the other segments, it is $x_2/\Delta C_2 = 5.33$ km/(Ah), $x_3/\Delta C_3 = 5.33$ km/(Ah), and $x_4/\Delta C_4 = 4.66$ km/(Ah). Results are reported in Fig. 7 (see the circle markers, representing experimental data).

An exponential function is used to fit experimental data points, namely

$$(x/\Delta C)\,(U) = r_1 \exp(r_2\, U) + r_3 \exp(r_4\, U)$$

where $r_1 = 6.873$, $r_2 = -0.06224$, $r_3 = -6.873$, and $r_4 = -1.28$ (see the solid line in Fig. 7). The fitting function shows a maximum for $U^\star = 2.5$ m/s (3.3% higher than the value estimated by battery model), where $(x/\Delta C)^\star = 5.60$ km/(Ah). Multiplying the specific range at that point by the total available capacity $C = 0.8\, C_0 = 0.8 \cdot 5.4 = 4.32$ Ah, one obtains $x^\star = 24.21$ km, as properly estimated by battery model.

4.3. Apollo Lunar Roving Vehicle: Simulation Results

The Lunar Roving Vehicle (LRV), visible in Fig. 8, is a four-wheel electric vehicle designed to operate in the low-gravity vacuum of the Moon and to be capable of traversing the lunar surface, allowing the astronauts of the last three Apollo missions to extend the range of their surface Extra Vehicular Activities (EVAs). On each mission, the LRV was used on three separate EVAs, for a total of nine lunar traverses. In what follows, the analysis will be focused on the Apollo 15 mission, that provided a greater opportunity

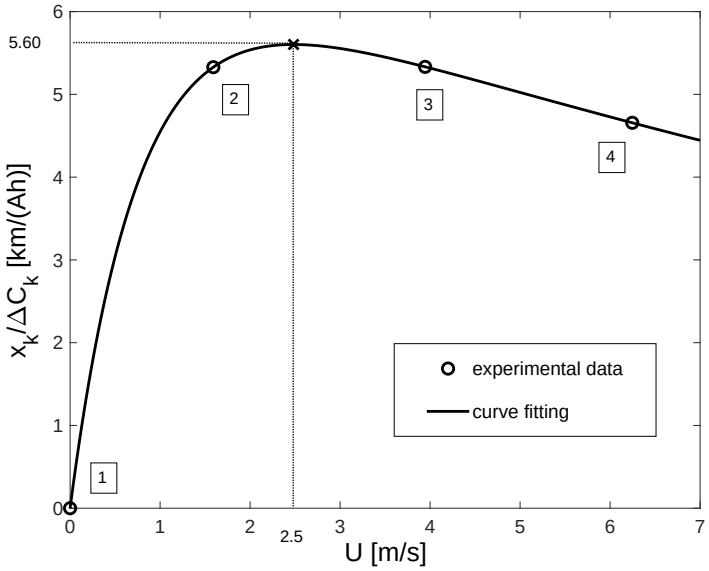

Figure 7: Experimental results (terrestrial rover): specific range as a function of speed.

for the study of the physical and mechanical properties of the lunar surface than any other previous mission. The LRV has a mass of 210 kg and was

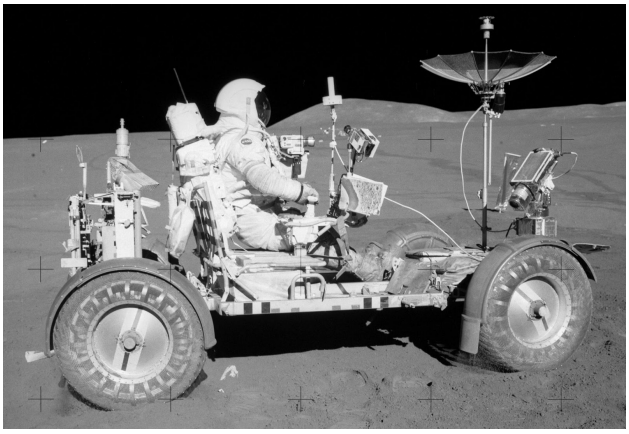

Figure 8: Commander David Scott drives the LRV near the Apollo 15 Lunar Module Falcon (courtesy of NASA).

designed to hold a payload of an additional 490 kg on the lunar surface, including two astronauts. Each wheel has its own electric drive, a DC series

wound 0.25 hp (186.5 W) motor capable of 10 000 rpm, attached to the wheel via an 80 : 1 harmonic drive with no gear shifting, and a mechanical brake unit. Maneuvering capability is provided through the use of front and rear steering motors. Each series wound DC steering motor is capable of 0.1 hp (74.6 W). Main power is provided by two 36 V silver-zinc potassium hydroxide non-rechargeable batteries with a capacity of 121 Ah, while the Lunar Communication Relay Unit is powered by a dedicated 400 Wh battery [36]. Passive thermal controls keep the batteries within an optimal temperature range (4 and 52°C).

No atmosphere characterizes the lunar environment, such that $\rho = 0$ kg/m^3 and there is no aerodynamic force opposing the vehicle motion. On the other hand, particular attention is required to analyze the interaction between the LRV and the lunar surface. In support of the Apollo soil mechanics investigations, extensive lunar soil simulation studies were conducted, based on data from Apollo 11 mission. In parallel with these investigations, extensive analyses were performed from photographic data obtained by the U.S. Lunar Orbiter Spacecraft programs [37] and in-place soil mechanics data obtained by the U.S.S.R. Luna spacecraft missions [38]. From these studies, the lunar surface was subdivided into four main categories - Smooth Mare, Rough Mare, Hummocky Uplands, and Rough Uplands. Based on power spectral density estimates, the parameter $\bar{k}_r$, which accounts for damper losses in Eq. (11), varies between 17.5 and 300. For the analysis of EVAs performed during the Apollo 15 mission, the roughness coefficient is selected as $\bar{k}_r = 17.5$ (Smooth Mare low range traverses).

The mechanical properties of lunar soils are remarkably similar to those

of terrestrial granular soils of comparable gradation, although the chemical composition of the two soil types may be dissimilar. The mechanical behavior of lunar soils appears to be dominated by the particle size distribution, particle shape, and packing characteristics (density, void ratio). In particular, quantitative measurements of the soil mechanical properties at the Apollo 15 site indicate that the soil conditions are variable on a regional basis, in accordance with pre-mission estimates for the LRV behavior, based on wheel-soil interaction tests performed on a wide spectrum of lunar soil simulants, under 1/6-g gravity conditions [30]. According to post-mission analyses, the soil model which yields the least percent deviation of estimated performance from effective LRV performance is Soil B in Table 7 of Ref. [30].

A vehicle mass $M = 626$ kg is considered, corresponding to weight $W = M\,g = 1\,017$ N (228.69 lb), where $g = 1.625$ m/s^2 is the gravity acceleration on the Moon. The parameters for the "Bekker/LLD soil-vehicle model C_w" and for the internal rolling resistance are reported in Table 6, from which one derives the soil consistency coefficient, $k = k_c/d + k_\phi = 3.0292$ lb/in^3, and the wheel sinkage, $z = 0.3$ in, according to Eq. (8).

Starting from the analysis of the torque generated by the single DC motor to allow vehicle motion at constant speed [30], the propulsive efficiency is estimated as $\eta_{prop} = 0.40$, with negligible variation over the design LRV speed range, restricted to 13 km/h (although a top speed of 18 km/h was recorded during the Apollo 17 mission). The efficiency of the PMU is estimated to be $\eta_{pmu} = 0.8$, which also includes cable losses. The total power absorbed by auxiliary systems include the contributions given by the Signal Processing Unit (SPU), the Directional Gyro Unit (DGU), and

Table 6: Rolling resistance parameters according to Soil B Bekker/LLD soil-vehicle model C_w.

Parameter	Symbol	Value	Units
External rolling resistance			
Wheel footprint area	S	62	in^2
Tire width of ground contact	d	6.85	in
Exponent of soil deformation	m	1	
Cohesive modulus of soil deformation	k_c	0.2	lb/in^{m+1}
Frictional modulus of soil deformation	k_ϕ	3	lb/in^{m+2}
Internal rolling resistance			
Zero-order rolling coefficient	μ_0	0.01	
First-order rolling coefficient	μ_1	$3.6 \cdot 10^{-4}$	s/m

the Integrated Position Indicator (IPI) [7]. After the LRV starting procedure, requiring about 3 min at a higher battery discharge rate, P_{aux} stabilizes at the value of approximately $40 + 16 = 56$ W, where 16 W is the total power required by the electronic speed controllers of the four traction motors. For a vehicle in motion, the gross power delivered from the PMU to the steering system according to Fig. 2, is directly estimated as $P_{st}(U)/\eta_{eps} = (P_{st0} + P_{st1}\,U)/\eta_{eps} = N_{st} \cdot Wa \cdot 74.6 - 3.5\,U$ W, where N_{st} is the number of active steering motors and 74.6 W is the maximum electrical power absorbed by the single electric actuator. The parameter $0 < Wa \leq 1$ is an empirical factor that accounts for a percent usage of maximum steering power at very low speed and includes a wander effect, determined by LRV path deviations in the presence of obstacles and driving errors. In addition, based on the trend analysis in [31], the power delivered to the servo-motors reduces by 3.5 W for every m/s. After checkout of the Apollo 15 LRV, it was

found that front steering mechanism was inoperative, such that EVA I was performed with only the rear steering actuators active ($N_{st} = 2$). During EVA II and III, instead, full steering was recovered ($N_{st} = 4$). A likely 30% usage of available steering power at low speed ($Wa = 0.3$) is assumed for EVA I and III, where frequent path deviations occurred with similar wandering activity. According to Ref. [39], EVA II was characterized by a smoother direct route, with about one fourth ($Wa = 0.075$) of the required steering effort that characterized EVA I and III.

In the absence of additional information, battery parameters are evaluated on the basis of the results in [23], where rechargeable lithium polymer (Li-Po) cells are analyzed. Note that a single Li-Po cell has a voltage of 4.2 V when fully charged and a nominal voltage $V_0 = 3.7$ V at the end of a safe discharge process. Hence, in order to satisfy the electrical standards of the LRV, based on a 36 V battery bus, a pack of 9 series-connected Li-Po cells ($9S$ configuration) is here considered, providing a voltage between 37.8 and 33.3 V during discharge. By extrapolating the data in [23] for a $9S$ battery, the following parameters are obtained at the reference temperature of 23°C: $\delta = 33.8$, $\epsilon = -1.025$, and $\beta = 0.9664$.

In Table 7 the three EVAs performed during the Apollo 15 mission are analyzed. For each EVA, $\bar{U}$ represents the average speed, obtained from the odometer reading at the end of the traverse divided by the ride time; $\bar{\gamma}$ is the average slope angle, weighted on the effective time spent while climbing, descending or driving on a flat surface; x is the odometer distance. Given the power profile parameters as obtained from Eq. (22), the discharged capacity C_{model} is estimated from the model in Eq. (26) with $U = \bar{U}$ and compared

to the LRV ampere-hour integrator readouts. Compared to the results avail-

Table 7: Comparison of measured and computed Apollo 15 LRV energy consumption (Soil B).

EVA	traverse characteristics			power coefficients				discharged capacity		
	$\bar{U}$ [m/s]	$\bar{\gamma}$ [deg]	x [km]	p_0	p_1	p_2	p_3	C_{model} [Ah]	C_{meas} [Ah]	error [%]
1	9.50	0.00	10.3	125.95	80.87	12.22	0	17.4	17.5	-0.6
2	9.15	0.23	12.5	97.98	93.63	12.22	0	21.6	20.5	+5.4
3	8.75	0.33	5.1	181.90	99.18	12.22	0	10.8	11.4	-5.3

able in Table 5 of Ref. [30], it can be noted that the estimation of discharged capacity by Eq. (26) is in closer agreement with the measured current consumption. In particular, the estimation error remains bounded below 6% for all EVAs (with respect to the median deviation as high as 30% in [30]), with a maximum overestimation error in EVA II.

Remark 2 Although the level of agreement between the computed and measured energy losses is considered to be very satisfactory, there are various uncertainties and error sources that may account for these discrepancies. These include: a) errors in the ampere-hour integrator and odometer readouts; b) errors in post-mission estimates of the slope distribution at the Hadley-Apennine region; c) errors in estimating the energy consumed by the navigation system, steering, control and display console, and other components, or activities not related to the traction-drive system; d) uncertainty in the estimation of soil characteristics; e) errors related to the parametrization of battery model. With respect to point d), methods for predicting terrain-shearing parameters online are available in recent literature [40], to be used in future missions for optimal route planning and traction control purposes. In this way, the traversability prediction and the determination of optimal driving strategies could be updated in real-time with no prior knowledge of

vehicle-soil interaction parameters. With respect to point e), it is worth noting that provided battery model parameters are derived from experimental data, originally obtained in [23] for an initial battery temperature of 23°C. According to the analysis in [39], the temperature inside the battery control units before each EVA ranged between 18°C and 36°C. In particular, at the beginning of the first traverse, battery temperature actually was 23°C. As a final consideration, note that wheel slip is not accounted for by the analysis of wheel-soil interaction in Section 2. Wheel slip may, for example, affect odometer accuracy and determine performance degradation. However, for low slope angles, LRV crew detected no wheel slip on Moon. This is not surprising because, from terrestrial experience, a wheel slip of less than about 20% is not detectable by the vehicle driver. From ad hoc wheel-soil interaction tests it was then estimated that effective wheel slip was less than $2-3\%$ on flat Moon surfaces. Hence, it is disregarded in this framework.

Consider the traverse parameters described in the first line of Table 7, where EVA I is analyzed with Soil B model. The total power required from the battery in a steady speed condition on a flat surface is plotted in Fig. 9 as a function of speed (see black symbols). Estimated range as given by Eq. (25) is also reported for $C = C_{model} = 17.4$ Ah. A best range condition exists, where $U_{br} = 11$ km/h, $P_{bbr} = 487.1$ W, and $x_{br} = 10.34$ km. It can be noted that U_{br} lies outside of the operative LRV speed range. As a matter of fact, the maximum is "flat", meaning that large variations of LRV speed are necessary for locally marginal gains in terms of expected range. Results are also provided, in the same plot, for a different selection of soil model parameters, representative of regional variations of soil mechanical

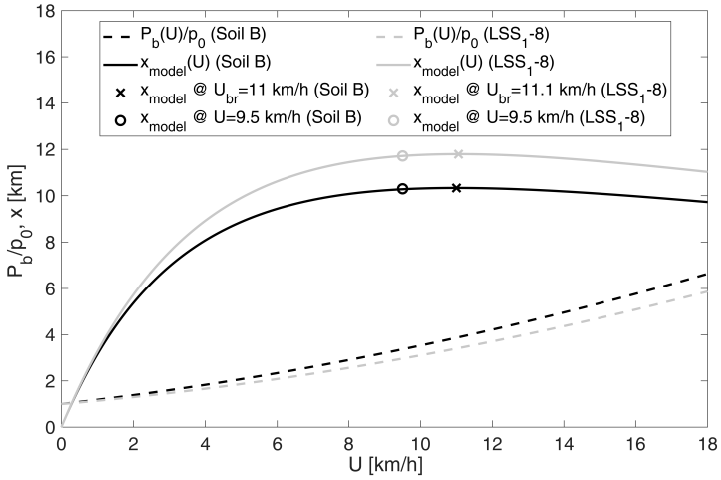

Figure 9: LRV performance during EVA I for different soil models.

properties (see gray symbols). In such a case, valid for Soil LSS_1-8, wheel sinkage reduces to $z = 0.18$ in and a performance improvement occurs for the same current consumption. The best range speed remains substantially unaltered ($U_{br} = 11.1$ km/h), while battery power reduces to $P_{bbr} = 432.0$ W, and the best range increases to $x_{br} = 11.8$ km. Finally, if $U = 9.5$ km/h, as in EVA I, the range becomes $x = 11.72$ km.

5. Conclusions

Performance of an electrically-powered exploration rover is discussed by means of a novel integral formulation for constant-power battery-discharge process. Performance is analyzed as a function of cruise speed and the best range driving strategy is identified as a function of relevant vehicle parameters, soil mechanical properties, and atmospheric data. Results are compared with those available in the literature, based on constant-current discharge models, and validated by numerical simulations and experimental tests on a small-size terrestrial rover powered by Li-Po batteries.

Particular attention is given to the application of the proposed method to performance analysis of the Lunar Roving Vehicle, used in the last three Apollo missions for Moon surface exploration. Based on available vehicle data, post mission analysis, and a detailed characterization of lunar soil mechanical properties, the required battery power is accurately evaluated as a function of speed for the different Extra Vehicular Activities performed during the Apollo 15 mission.

The principles developed for the determination of best-range conditions are of general validity. Hence, the effectiveness of the proposed approach and the simplicity of the experimental setup prove to be encouraging for improving the preliminary sizing methods of electrical vehicles of any size and task for future missions, under the assumption of constant speed.

References

[1] R.A. Yingst, et al., Testing the efficiency of rover science protocols for robotic sample selection: A GeoHeuristic Operational Strategies Test, Acta Astronautica 146 (2018) 300-315, https://doi.org/10.1016/j.actaastro.2018.02.029

[2] J. Jiang, et al., Path planning for asteroid hopping rovers with pretrained deep reinforcement learning architectures, Acta Astronautica 171 (2020) 265-279, https://doi.org/10.1016/j.actaastro.2020.03.007

[3] N. Patel, R. Slade, J. Clemmet, The ExoMars rover locomotive subsystem, J. Terramechanics 47 (2010) 227-242.

[4] Y. Zhao, et al., A high-accuracy autonomous navigation scheme

for the Mars rover, Acta Astronautica 154 (2019) 18-32, https://doi.org/10.1016/j.actaastro.2018.10.036

[5] R. Welch, D. Limonadi, R. Manning, Systems engineering the Curiosity Rover: A retrospective, in: 8th International Conference on System of Systems Engineering (SoSE) (2013) 70-75, https://doi.org/10.1109/SYSoSE.2013.6575245

[6] F. Zhou, et al., Simulations of Mars Rover Traverses. J. Field Robotics 31(1) (2014) 141-160, https://doi.org/10.1002/rob.21483

[7] E.C. Smith, W.C. Mastin, Lunar Roving Vehicle Navigation System Performance Review, NASA TN 0-7469 (1973) 1-6.

[8] V. Asnani, D. Delap, C. Creager, The Development of Wheels for the Lunar Roving Vehicle, J. Terramechanics 46(3) (2009) 89-103, https://doi.org/10.1016/j.jterra.2009.02.005

[9] C. Sulzberger, An early road warrior: electric vehicles in the early years of the automobile, IEEE Power and Energy Magazine 2(3) (2004) 66-71, https://doi.org/10.1109/MPAE.2004.1293606

[10] M. Kamali, et al., Formal verification of autonomous vehicle platooning. Sci. Computer Programming 148 (2017) 88-106, https://doi.org/10.1016/j.scico.2017.05.006

[11] M. Mruzek, et al., Analysis of parameters influencing electric vehicle range, in: 9th International Scientific Conference (Transbaltica 2015) 134, 165-174, https://doi.org/10.1016/j.proeng.2016.01.056

[12] P. Dost, P. Spichartz, C. Sourkounis, Cost efficiency of electric vehicles and extended range electric vehicles for various user groups, in: International Symposium on Power Electronics, Electrical Drives, Automation and Motion (2015) 1220-1225, https://doi.org/10.1109/SPEEDAM.2016.7526009

[13] D. Perrotta, et al., On the Potential of Regenerative Braking of Electric Buses as a Function of Their Itinerary, Procedia - Social and Behavioral Sciences 54 (2012), 1156-1167, https://doi.org/10.1016/j.sbspro.2012.09.830

[14] G. Le Solliec, A. Chasse, M. Geamanu, Regenerative braking optimization and wheel slip control for a vehicle with in-wheel motors, in: IFAC Proceedings Volumes 46(21) (2013) 542-547, https://doi.org/10.3182/20130904-4-JP-2042.00043

[15] G. Doukas, P. Bauer, J. van der Burgt, Battery operation cycle management for electric vehicles with battery switching technology, in: IEEE Transportation Electrification Conference and Expo (2014) 1-6, https://doi.org/10.1109/ITEC.2014.6861864

[16] D. Babu, A. Kumar, J. Roychowdhury, Energy aware battery powered electric vehicles: a predictive model driven approach, in: 2nd International Conference on Advances in Computer Science and Engineering (2013) 213-218, https://doi.org/10.2991/cse.2013.49

[17] H. Rahimi-Eichi, M.Y. Chow, Big-data framework for electric vehicle range estimation, in: 40th Annual Conference

of the IEEE Industrial Electronics Society (2014) 5628-5634, https://doi.org/10.1109/IECON.2014.7049362

[18] H. Rahimi-Eichi, F. Baronti, M.Y. Chow, Online adaptive parameter identification and state-of-charge coestimation for lithium-polymer battery cells, IEEE Transactions on Industrial Electronics 61(4) (2013) 2053-2061, https://doi.org/10.1109/TIE.2013.2263774

[19] W. Peukert, Über die Abhängigkeit der Kapazität von der Entladestromstärke bei Bleiakkumulatoren, Elektrotechnische Zeitschrift 20 (1897) 20-21.

[20] I.J.M. Besselink, et al., Design of an efficient, low weight battery electric vehicle based on a vw Lupo 3l, in: 25th World Battery, Hybrid and Fuel Cell Electric Vehicle Symposium & Exhibition (2010) 1-10.

[21] K. Vatanparvar, J. Wan, M.A. Al Faruque, Battery-aware energy-optimal electric vehicle driving management, in: IEEE/ACM International Symposium on Low Power Electronics and Design (2015) 353-358, https://doi.org/10.1109/ISLPED.2015.7273539

[22] C.M. Shepherd, Design of primary and secondary cells - An equation describing battery discharge. J. Electrochemical Society 112(7) (1965) 657-664, https://doi.org/10.1149/1.2423659

[23] G. Avanzini, E.L. de Angelis, F. Giulietti, Optimal performance and sizing of a battery-powered aircraft, Aerosp. Sci. Technol. 59 (2016) 132-144, https://doi.org/10.1016/j.ast.2016.10.015

[24] M.E. Fuller, A Battery Model for Constant-Power Discharge Including Rate Effects, Energy Conversion and Management 88 (2014) 199-205, https://doi.org/10.1016/j.enconman.2014.08.015

[25] S. Jiang, et al., Adaptive estimation of road slope and vehicle mass of fuel cell vehicle, eTransportation 2 (2019) 1-9, https://doi.org/10.1016/j.etran.2019.100023

[26] V.R. Tannahill, K.M. Muttaqi, D. Sutanto, Driver alerting system using range estimation of electric vehicles in real time under dynamically varying environmental conditions, IET Electrical Systems in Transportation 6(2) (2016) 107-116, https://doi.org/10.1049/iet-est.2014.0067

[27] G.C. Birur, et al., Thermal Control of Mars Lander and Rover Batteries and Electronics Using Loop Heat Pipe and Phase Change Material Thermal Storage Technologies, TP 2000-01-2403, in: International Conference On Environmental Systems (2000) 1-10, https://doi.org/10.4271/2000-01-2403

[28] W.H. Press, et al., Numerical recipes: the art of scientific computing - 2nd Edition, Cambridge University Press (1992) Chs. 5, 9, and 10.

[29] R.P. Brent, Algorithms for minimization without derivatives, Prentice-Hall (2013) Ch. 5.

[30] N.C. Costes, J.E. Farmer, E.B. George, Mobility performance of the Lunar Roving Vehicle: terrestrial studies - Apollo 15 results, NASA TR R-401 (1972) 1-86.

[31] J. Zhao, et al., Design and Full-Car Tests of Electric Power Steering System. Computer and Computing Technologies in Agriculture 1, Springer (2008) 729-736, https://doi.org/10.1007/978-0-387-77251-6_80

[32] M. Ehsani, et al., Modern electric, hybrid electric, and fuel cell vehicles, Power electronics and application series, CRC Press LLC (2005) 22-27.

[33] A.A. Rula, C.J. Nuttall Jr., An Analysis of Ground Mobility Models - ANAMOB, Technical Report No. M-71-4, U.S. Army Engineer Waterways Experiment Station, Vicksburg, Miss. (1971) 1-238.

[34] L. Schirone, M. Macellari, Design Issues for the Design of a Lunar Rover, ESA SP-719, in: 10th ESPC (European Space Power Conference) (2014) 1-5.

[35] D. Curtiss, Recent extensions of Descartes' rule of signs, Annals of Maths 19(4) (1918) 251-278.

[36] LCRU Program Management Office, Crew Training Manual Lunar Communications Relay Unit, LRTM-SY-1 Rev. D (1971) 3-9.

[37] N.C. Costes, G.T. Cohron, D.C. Moss, Cone Penetration Resistance Test - An Approach to Evaluating the In-Place Strength and Packing Characteristics of Lunar Soils, in: Proceedings of the Second Lunar Science Conference Vol. 3, MIT Press (1971) 1973-1987.

[38] J.K. Mitchell, et al., Mechanical Properties of Lunar Soil: Density, Porosity, Cohesion, and Angle of Internal Friction, in: Proceedings of the Third Lunar Science Conference Vol. 3, MIT Press (1972) 3235-3253.

[39] Saturn Flight Evaluation Working Group, MPR-SAT-FE-71-2, Saturn V Launch Vehicle Flight Evaluation Report AS-510 Apollo 15 Mission (1971) 278-281.

[40] L. Xue, et al., In situ identification of shearing parameters for loose lunar soil using least squares support vector machine, Aerosp. Sci. Technol. 53 (2016) 154-161, https://doi.org/10.1016/j.ast.2016.03.018